COBEM 2023 27TH INTERNATIONAL CONGRESS OF MECHANICAL ENGINEERING

ABCM Brazilian Society of Mechanical Sciences and Engineering
27th ABCM International Congress of Mechanical Engineering
December 04-08, 2023, Florianópolis-SC, Brazil

COB-2023-0828
TENSILE STRENGTH SPECIMENS FOR NON-SOLID BLOCK SUPPORT STRUCTURES MANUFACTURED BY LASER POWDER BED FUSION: A PRELIMINARY STUDY

Dan Alexander Gallego[a,b]
Henrique Rodrigues Oliveira[a]
Insituto SENAI de Inovação em Processamento a Laser[a]
dan.gallego@sc.senai.br[a], henrique.oliveira@sc.senai.br.

Neri Volpato[b]
Universidade Tecnológica Federal do Paraná, Núcleo de Manufatura Aditiva e Ferramental – NUFER[b].
nvolpato@utfpr.edu.br[b]

Abstract. *Metal Laser-based Powder Bed Fusion (L-PBF) is a prominent category within Additive Manufacturing (AM), offering numerous advantages over traditional manufacturing techniques, including the ability to create complex geometries, produce items on demand, consolidate parts, improve energy efficiency, and reduce lead time. However, L-PBF also faces challenges, such as low productivity, inferior surface roughness, limited dimensional accuracy, and the need for support structures for overhang surfaces. Support structures in L-PBF are essential for enhancing heat dissipation, anchoring the part to the substrate, and reducing residual stress during printing. Despite their significance, limited research has been conducted on this subject. This paper provides an overview of different types of support structures and design aspects. The feasibility of manufacturing samples for tensile strength testing of non-solid block-type support structures based on the ASTM E8/E8M–16a standard was studied. Then, the impact of laser power and scanning speed on the consolidation interface between part and support was also investigated. Understanding and optimizing the processing of support structures can increase productivity, reduce manufacturing costs, minimize printing risks, and guarantee the repeatability of the designs. This research contributes to further advancements in designing support structures in L-PBF, making it a more efficient and reliable technique.*

Keywords: *additive manufacturing, selective laser melting, directed metal laser sintering, support structure, AISI 316L stainless steel.*

1. INTRODUCTION

According to the ISO/ASTM 52900:2015 standard, *Powder Bed Fusion (PBF) is an Additive Manufacturing (AM) process where thermal energy selectively melts regions of the powder bed.* The PBF process is categorized based on the energy source used to process the raw material and the type of material it consists of. There are three categories divided according to the energy source used in the process: Electron Beam (EB), Infrared Light (IRL), and Laser (L). Concerning the feedstock material, PBF usually processes metals, polymers, ceramics, and composites.

As reported by DebRoy *et al.* (2018), the metal Laser-based Powder Bed Fusion (L-PBF) method has gained prominence in the industry due to its ability to produce customized and complex parts that would be challenging or even impossible to obtain through traditional manufacturing techniques. This design freedom provided by the technology allows for a reduction in the number of parts needed to assemble a system, eliminating post-processing steps and reducing delivery time (Bayoumi, 2000). Moreover, L-PBF enables on-demand manufacturing of parts, ensuring the continuous operation of critical systems without the need for spare part inventory. These advantages have drawn the attention of several industrial sectors that develop high-value-added products, such as aerospace, biomedical, dental, energy, oil and gas, defense, and automotive industries. The L-PBF method's capabilities make it a compelling choice for these sectors, offering increased efficiency, cost-effectiveness, and the ability to meet specific and complex design requirements.

Volpato and de Carvalho (2017) mention some advantages that processing through L-PBF can bring compared to traditional manufacturing processes, such as geometric freedom, minimal material waste, efficient energy utilization, rapid prototyping, and on-demand production, eliminating the need for inventory storage. Regarding disadvantages, one can mention anisotropic mechanical properties, lower dimensional accuracy and surface finish, limited material diversity, low productivity, high production costs, the requirement for support structures, and the adoption of excess material for post-processing (Oliveira *et al.*, 2020). Despite these drawbacks, as research progresses, a deeper understanding of the technology is achieved, leading to the overcoming of these challenges. Hence, the importance of studying and researching this technology.

Figure 1 illustrates a schematic representation of the L-PBF technique. The process starts with the deposition of the first metal powder layer by the spreader blade onto a substrate, which is assembled on the L-PBF building platform. After the first layer is deposited, the laser is activated and directed by a galvanometer mirror system. The laser beam selectively scans an area, melting the layer's particles onto the substrate. Upon completion of the scan, the build platform moves downward a distance corresponding to the layer thickness, while the deposition platform moves upward to deposit the next layer of powder. The powder deposition is typically controlled to cover the entire bed surface through the spreader's distribution, and an overflow platform collects any overspreading. This process is repeated successively, with each layer being fused onto the underlying layers until the final building model is concluded (Volpato and de Carvalho, 2017). According to the ISO/ASTM 52921:2013 standard, the direction z always refers to the build direction, while the xy plane is parallel to the substrate. It is important to note that the machine's architecture may vary depending on the manufacturer.

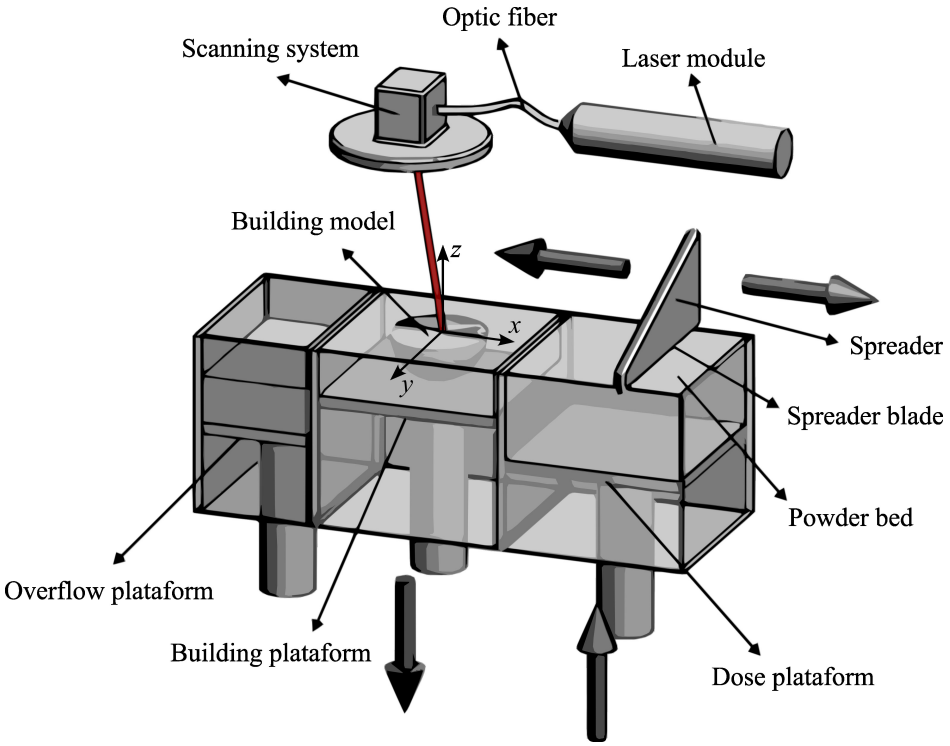

Figure 1. Schematic representation of an L-PBF processing, adapted from Aulus and Bineli (2011).

Due to the complexity of L-PBF technology, AM system suppliers focusing on metal materials have developed sets of processing parameters for each application case. In modern systems, there can be more than 100 processing parameters, which are currently optimized numerically and/or empirically (Oliveira *et al.*, 2020). Usually, these formulations aim to minimize defects produced during processing and maximize performance in terms of production and quality. However, given the technology's significant design freedom, it is impossible to develop a single methodology that optimizes these processing parameters for all characteristics of manufactured parts, such as thin walls, thick sections, overhung surfaces, and lattice structures.

In this way, these parameters can be configured to achieve the desired properties of the processed materials, such as tensile strength, impact resistance, fatigue resistance, corrosion resistance, surface roughness, microstructure characteristics, porosity, hardness, dimensional accuracy, among others (Oliveira *et al.*, 2020). To achieve this, there are strategies and approaches with specific sets of parameters for the volume (bulk) and surface (contour) of the part, as well as for the support structures (Bassoli *et al.*, 2018). By fine-tuning these parameters, manufacturers can optimize the production process and achieve the desired material properties, ensuring high-quality parts that meet the specific requirements of different applications.

The ability to control and adjust these parameters based on the characteristics of the parts being produced allows for greater flexibility in the AM process. It opens up possibilities for a wide range of applications across various industries. In the literature, several studies investigate methodologies to define processing windows and strategies for bulk and contour regions, aiming to mitigate defects and optimize the productivity of the processed part. The bulk processing window refers to the set of parameters that process the solid regions of the part, as the contour processing window refers to the surface of the part (Tan *et al.*, 2019; Oliveira *et al.*, 2020; Liu *et al.*, 2021). However, methodologies that search processing parameters for support structures have been neglected and are scarce in the literature (Jiang *et al.*, 2018). As a result, there is a need for more research focused on finding the most suitable processing parameters for support structures.

Thus, these studies could help improve the overall quality, stability, and success rate of L-PBF manufacturing processes by ensuring proper support structure design and processing. Additionally, as reported Weber *et al.* (2020), one of the most common problems identified during L-PBF manufacturing is the processing or design of support structures. This issue occurs mostly because those responsible for their designing/processing underestimate their importance. Figure 2 shows an application of design for additive manufacturing using L-PBF. In this study, a filler breather was redesigned and fabricated respecting L-PBF processing constraints, however, some support structure issues were reported (Gallego *et al.*, 2022). Further complications in the support structures could compromise the entire build. Despite that, the build was finished successfully.

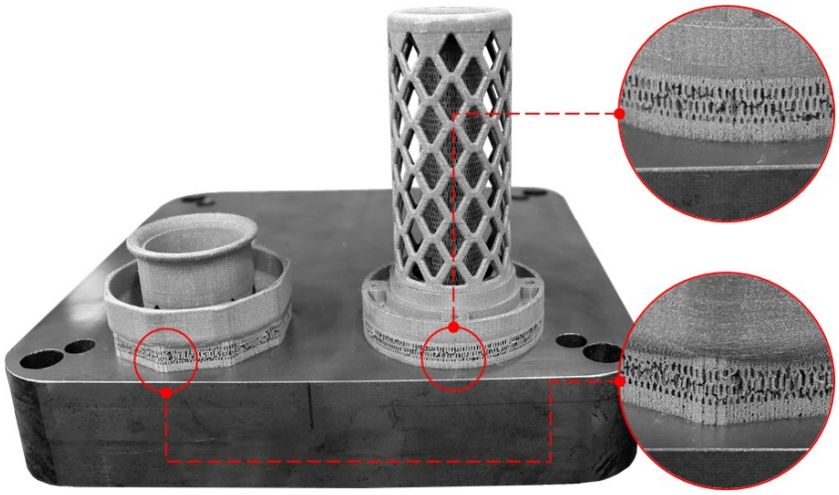

Figure 2. Filler breather build with support structures issues (Gallego *et al.*, 2022).

Searching in the SCOPUS database for scientific articles published between 2000 and 2022, using the keywords "Laser Powder Bed Fusion" combined with the "OR" operator and common names such as "LaserCUSING", "Direct Metal Laser Sintering", and "Selective Laser Melting" (Munhoz *et al.*, 2017) yielded a total of 16.290 publications. When this result was combined with the terms "support structure" and "support material" using the "AND" operator, the new result yielded 244 publications. As shown in Fig. 3, it can be observed that while the number of publications related to the L-PBF has grown rapidly in recent years when combined with "support structure" terms, the growth rate s is irrelevant. It is noted that the total of publications on the topic "L-PBF" combined with "support structures" terms represent only 1,5% of the total publications with the single term "L-PBF".

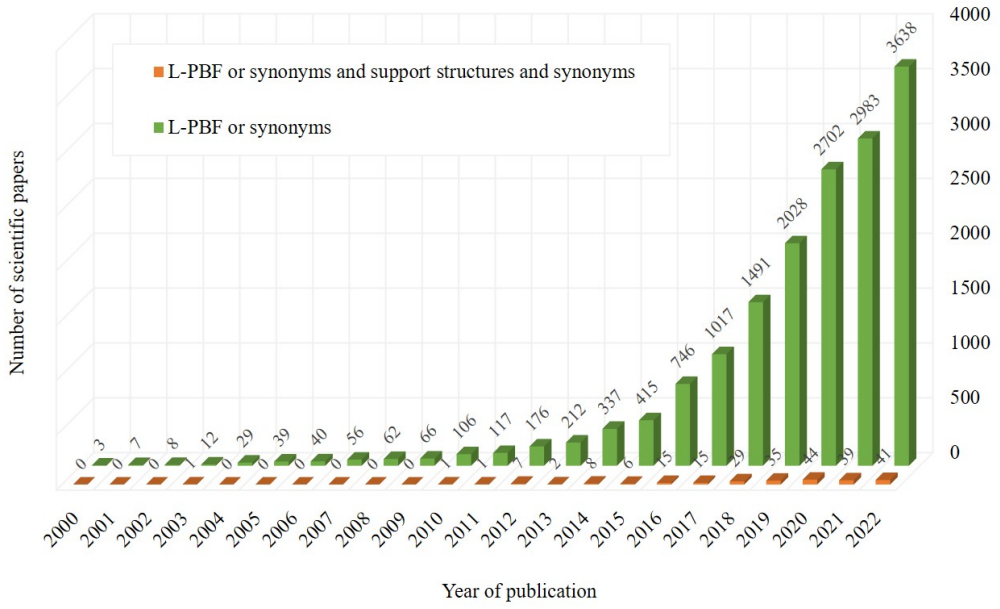

Figure 3. Comparison of the number of scientific articles published from 2000 to 2022 using the term *L-PBF* "OR" similar vs. the term *L-PBF* "OR" similar "AND" *support structures* "OR" *support material*.

2. LITERATURE REVIEW

In L-PBF, the implementation of support structures is necessary when there are overhung surfaces in the building model. According to Calignano (2014), an *overhanging structure* is defined as *a region of the manufactured part that is not built on a platform or underlying melted layers*. These regions are critical and must be carefully planned as they risk collapsing during fabrication. They can be self-supporting; the maximum angle that distinguishes a region as self-supporting or not is called *self-supporting angle* or *maximum overhanging angle*, which is typically defined as θ_c = 45 degrees concerning the building direction z (Wang *et al.*, 2012). Figure 4 shows the manufacturing of a suspended structure for different inclinations, along with the representation of the 3D model of the part. It can be observed that as the inclination angle decreases, the surface roughness of the suspended structure increases. In this example, the critical inclined angle θ_c for the construction to be viable is 30 degrees, since the structure collapses below that angle.

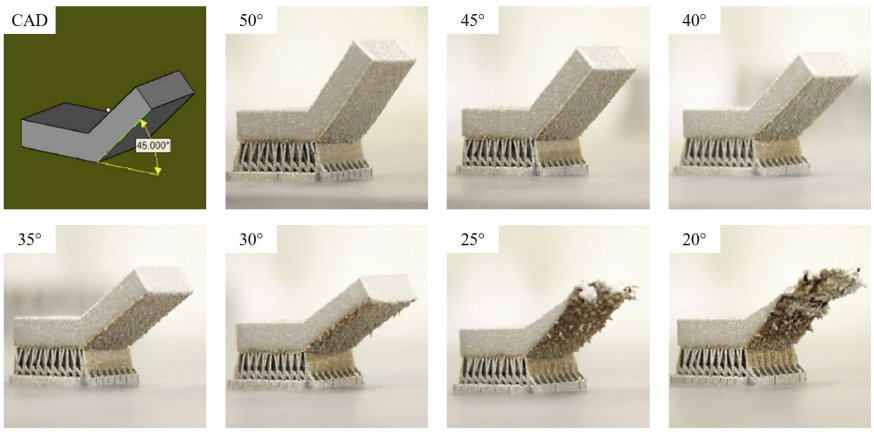

Figure 4. Different angles for overhanging structures (Zhu *et al.*, 2019).

As reported by Bartsch *et al.* (2020), support structures are divided into two categories: solid and non-solid. Solid support structures are supports formed by adjacent-continued scanning tracks, such as cones, pins, and heat sinks, while non-solid structures are structures made by one laser track such as block, point, contour, line, and web. In the literature, there are studies investigating the impact of two aspects on the quality of support structures in parts manufactured by L-PBF: processing parameters and geometric parameters. As mentioned by Weber *et al.* (2020), one of the difficulties faced by these studies lies in the lack of common objectives and standardized evaluation methods for comparison purposes.

Figure 5 summarizes the geometric parameters of block-type support structures relevant to this study. In Fig. 5 (a), block supports are made of a grid of lines in the xy plane, each separated by the same distance called hatching space h_s. On the same image, it is possible to observe the rotation angle ϕ, which defines the angle around the z direction. In Fig 5 (b) it is possible to see in the x/yz plane the offset from the edge of the part and the support contour $[xy]_o$, as well as the offset between the top and/or the bottom of the support and their respective surface $[z]_o$. Besides, it is shown a "perforation" feature, used mostly to facilitate powder removal. In this feature, s_h is the solid height, which is the distance between perforations and the part surface; s_p is the height of the perforation; b_p is the beam width of the perforation; and θ_p is the perforation angle.

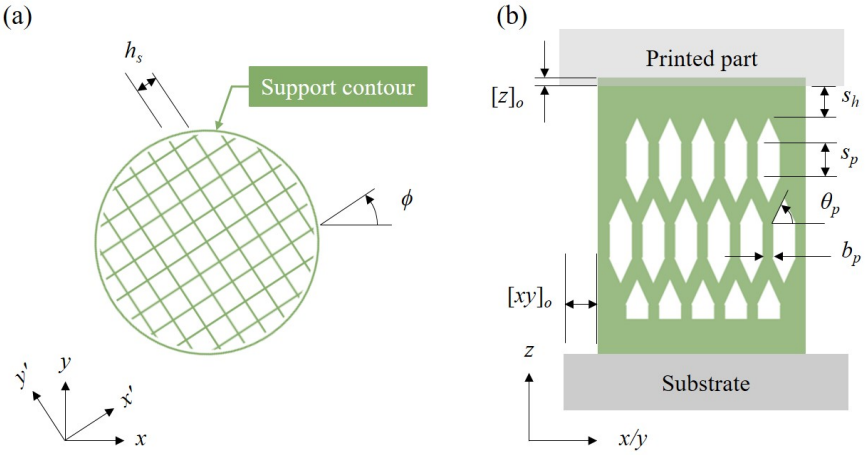

Figure 5. Design parameters of non-solid block supports: (a) xy plane; (b) x/yz plane, adapted from Schmitt *et al.* (2020).

Figure 6 illustrates some of the most relevant processing parameters during the selective laser melting of a single layer of a non-solid block-type support structure with thickness t. As shown, the laser beam with spot diameter d_s and power P scans the tracks with speed v, according to the predefined scan vector in the slicing step. Finally, w is the track width melted resulting from the laser beam scanning vector, and therefore it depends on P, v, and d_s (Tan *et al.*, 2019).

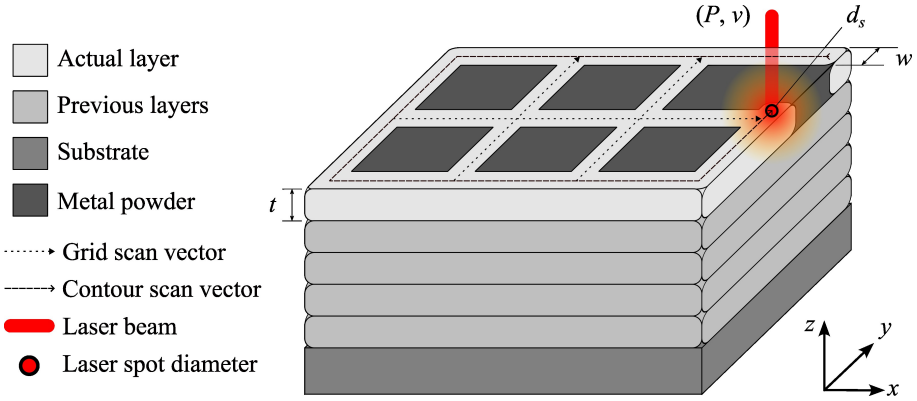

Figure 6. L-PBF processing parameters for non-solid block-type support structures.

One way to relate the most relevant processing parameters for L-PBF is through the volumetric energy density E_V (Sun *et al.*, 2017), as shown in Eq. 1. Some studies use the distance between scanning lines h_d instead of the diameter d_s (Sefene, 2022). The E_V has proven to be an empirical formulation in the relationship between these processing parameters for different materials processed by L-PBF, as it simplifies the energy fed into the system per unit volume. Because of that, the combination of different processing parameters that result in the same E_V values can lead to different results (Sun *et al.*, 2017). The E_V is obtained according to the equation

$$E_V = \frac{P}{d_s \times v \times t}. \tag{1}$$

In essence, support structures are used for fulfilling two main objectives: improving heat dissipation and anchoring it to the substrate to prevent warping and ensure dimensional stability, both caused by residual stresses and avoiding collapse during the laser fusion process (Munhoz *et al.*, 2017). Once the printing is completed, the powder trapped in the bed needs to be cleaned and the support structures need to be removed via manual or conventional machining methods in post-processing stages (Munhoz *et al.*, 2017). As a result, support structures are designed and processed with different objectives than the parts they support.

In the study reported by Calignano (2014), the impact of geometric parameters of the block-type support structure and their influence on warpage and ease of removal were investigated in AlSi10Mg and Ti6Al4V specimens, keeping processing parameters constant. The presence of perforation, as well as the parameters h_s and $[z]_o$ were evaluated, among other characteristics. The work concluded that the parameters h_s were both materials' most influential characteristics.

Bobbio *et al.* (2017) proposed a method to quantify the tensile strength of block-type support structures and compared it with the strength of solid structures of Ti6Al4V from other studies. The study concluded that the h_s and the height of the teeth (another geometric feature from block supports) were the most influential factors on the tensile strength. The specimens exhibited macroscopic brittle behavior, but microscopically, a ductile fracture mode was observed. Lindecke *et al.* (2018) and Leary *et al.* (2019) used the method proposed by Bobbio *et al.* (2017) and evaluated different aspects of block-type support structures applied to other materials and came to similar conclusions.

Schmitt *et al.* (2020) conducted the most recent study aiming to optimize support processing parameters experimentally for block-type support structures in 16MnCr6 specimens. The study aimed to achieve robustness against residual stresses by maximizing tensile strength and ease of removal by minimizing shear strength. The results indicated that P was the most influential parameter for shear strength, while t was the most influential for tensile strength.

One factor that has been discussed is the impact of the track width w on the mechanical resistance of non-solid block-type support structures. Recent works have used microscopy and tomography techniques to characterize the real sizing of w after processing and how to consider it in the mechanical resistance calculations (Lindecke *et al.*, 2018; Leary *et al.*, 2019). Furthermore, it is known that w has a direct relation with E_V, in such a way that when E_V increases, w increases as well; when E_V decreases, w also decreases (Tan *et al.*, 2019).

Overall, the literature review revealed the lack of standardization in test specimens and methods, which makes it difficult to compare the studies on this subject (Jiang *et al.*, 2018; Weber *et al.*, 2020). Based on this, a preliminary study was proposed in this work to develop a sample as per the ASTM E8/E8M–16a standard in AISI 316L. In addition, different combinations of laser power P and laser scanning speed v were tested to evaluate the impact of processing parameters on the quality of the interface between part and support.

3. MATERIALS AND METHODS

The feedstock material used for the experiments was AISI 316L stainless steel. This austenitic alloy is popularly used and highly processable by L-PBF technology. The chosen metal powder's particle size distribution is 20–53 µm atomized via gas. In this work, a layer thickness t of 60 µm for the AM processing was arbitrated.

The L-PBF equipment used for sample fabrication is the M2 Cusing from Concept Laser, currently GE Additive. The available volume in the build chamber is 245×245×285 mm³. The machine is capable of maintaining oxygen concentrations below 0,5% during fabrication. The system has a continuous emission Yd:YAG fiber laser with a wavelength of 1070 nm and a maximum P of 400 W. The configured focal diameter d_s for the laser is 100 µm. The scanning system consists of a set of galvanometer mirror arrangements, capable of achieving v of up to 7000 mm/s. The samples were fabricated on a substrate of AISI 316L stainless steel.

Based on the study presented by Denardi (2021) and using Eq. 1, a range of E_V from 24 to 50 J/mm³ was chosen. Therefore, considering v varying from 500 to 2100 mm/s with a 400 mm/s step, and P varying from 100 to 350 W with a 50 W step, 13 parameter combinations were selected. Table 1 shows the design parameters for the block-type support structure set constant and Tab. 2 shows the different combinations of processing parameters tested.

Table 1. Constant design parameters.

Parameter	Value	Reference
θ_p	60 deg	Software recommendation
ϕ	45 deg	Software recommendation
h_s	1,5 mm	Schmitt *et al.* (2020)
s_h	1,5 mm	Schmitt *et al.* (2020)
$[z]_o$	0	Lindecke *et al.* (2018)
$[xy]_o$	0	Author definition
b_p	0,4 mm	Lindecke *et al.* (2018)
s_p	1,0 mm	Schmitt *et al.* (2020)

Table 2. Variable processing parameters.

ID	P [W]	v [mm/s]	E_V [J/mm³]
1	100	500	33,3
2	150	500	50,0
3	150	900	27,8
4	200	900	37,0
5	250	900	46,3
6	200	1300	25,6
7	250	1300	32,1
8	300	1300	38,5
9	350	1300	44,9
10	250	1700	24,5
11	300	1700	29,4
12	350	1700	34,3
13	350	2100	27,8

The sample for the tensile test was designed based on the subsize ASTM E8/E8M–16a specimen, as Fig. 7 (a) shows. The building model was created in the Magics software, version 26.02, from Materialize, and it is exhibited in Fig. 7 (b) from a perspective view. The samples that corresponded to the processing parameter combinations were organized along the "+y" direction on the building plate (1–13). At the same time, the replicas were set along the "+x" direction (A, B, C, D, and E).

(a)

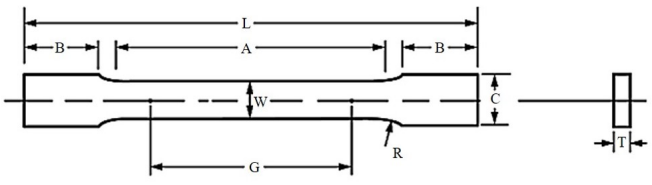

Symbol	Description	Value	Unit
G	Gauge length	25,0 ± 0,1	mm
W	Width	6,0 ± 0,1	mm
T	Thickness	6,0	mm
R	Radius of fillet	6,0	mm
L	Overall length	100	mm
A	Length of reduced parallel section	32	mm
B	Length of grip section	30	mm
C	Width of grip section	10	mm

(b)

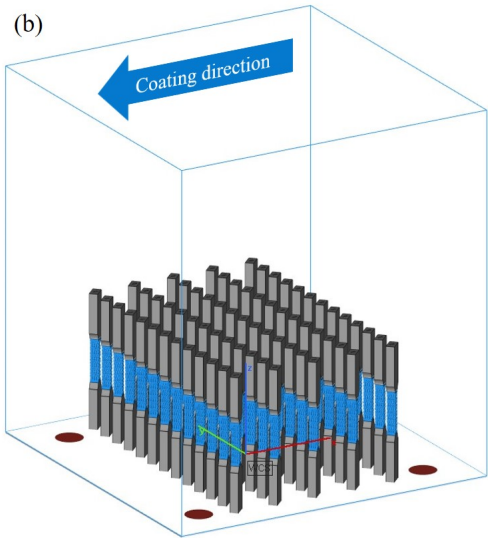

Figure 7. Manufacturing plan: (a) sample design and (b) view of the building model from perspective.

After manufacturing, the specimens were cut from the substrate using wire-electrical discharging machining (WEDM) and visually inspected. Next, the results were examined in a Carl Zeiss®stereoscope, model Discovery.V8, with magnifications ranging from 1,6 to 8,0 times.

4. PRELIMINARY RESULTS AND DISCUSSION

The L-PBF manufacturing and its result are shown in Fig. 8. Figure 8 (a) shows the laser processing from one of the layers. The highest oxygen level registered corresponded to 0,4% and the building concluded without any interruption. After removing the powder from the building chamber and the substrate from the building platform, it became evident that some samples exhibited consolidation issues at the lower interface between the solid region and the support structure, as indicated by the red markings in Fig. 8 (b). Then, the samples were removed from the substrate via WEDM.

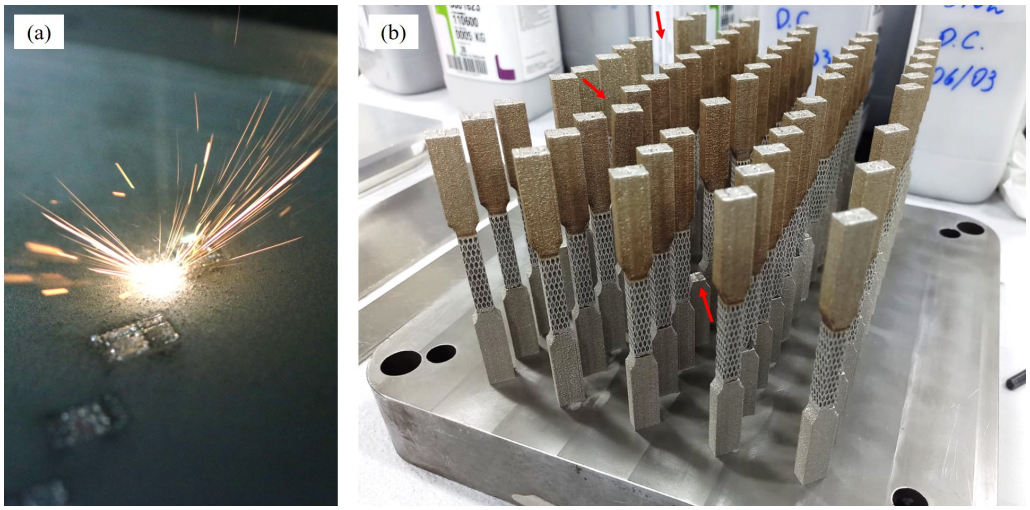

Figure 8. L-PBF manufacturing: (a) laser processing and (b) build concluded and cleaned.

It is possible to observe in Fig. 9 the contrast between the two extremes, both built with the lowest and the highest value of E_V with the building direction indicated. Figure 9 (a) depicts sample 2, which corresponds to E_V = 50,0 J/mm³, as Fig. 9 (b) depicts sample 10, which corresponds to E_V = 24,5 J/mm³. The replicas related to sample 2 did not present any apparent issue; however, 4 out of the 5 replicas of sample 10 displayed problems at the lower interfaces between the solid part and support. Similar problems were observed in other samples where values of E_V were lower than 34,3 J/mm³ (sample 12). Besides the consolidation problem, it is possible to note different colors between the upper and lower regions of all samples. The upper region exhibited a brownish color, indicating overheating, as the lower region exhibited a regular metallic aspect.

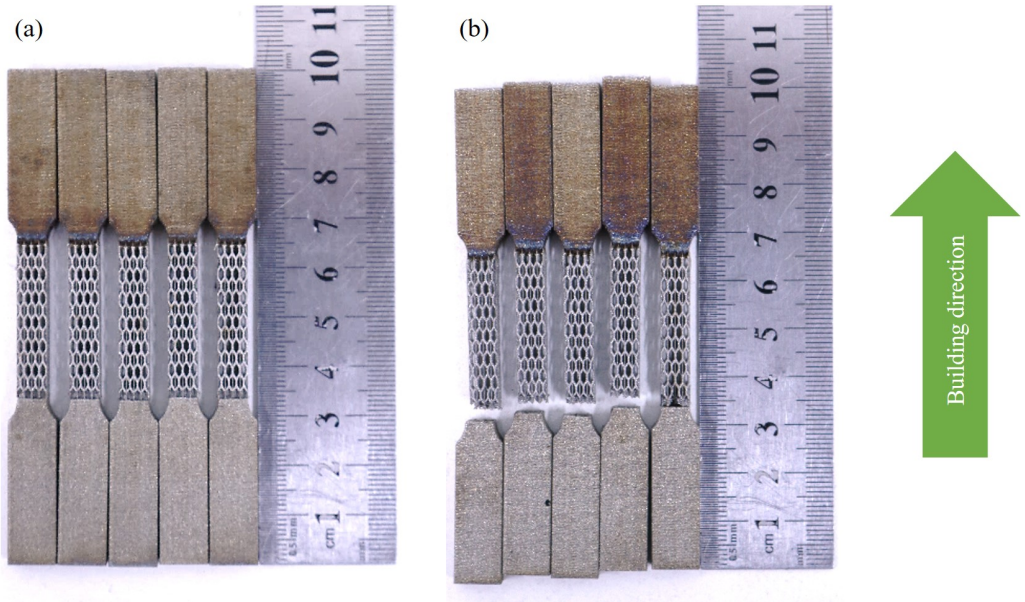

Figure 9. Contrast of the results: (a) sample 2 and (b) sample 10.

Figure 10 presents macrographs of sample 6, captured at a magnification of 1,6 times using a stereoscope. As previously discussed and now evidenced by Fig. 10 (a), consolidation issues manifested only at the lower interfaces. Even though the bottom solid region did not disconnect from the solid region, the failure in an eventual tensile test would occur in this interface due to the material discontinuity. Furthermore, overheating was observed between the specimen's support and solid upper interface, as indicated by the distinct coloration in the region highlighted by the dashed line in Fig. 10 (b). A shrinkage effect in the overheated region could be noticed as well, leading to the rupture of support contour beams, as indicated by the red arrow. Besides, since $[xy]_o$ was defined as 0 mm, it is possible that a portion of the support contour is being scanned out of the bulk region of the following layers that correspond to the upper solid part from the specimen. Lastly, Fig. 10 (c) depicts the intermediate support zone, where no issues have been detected.

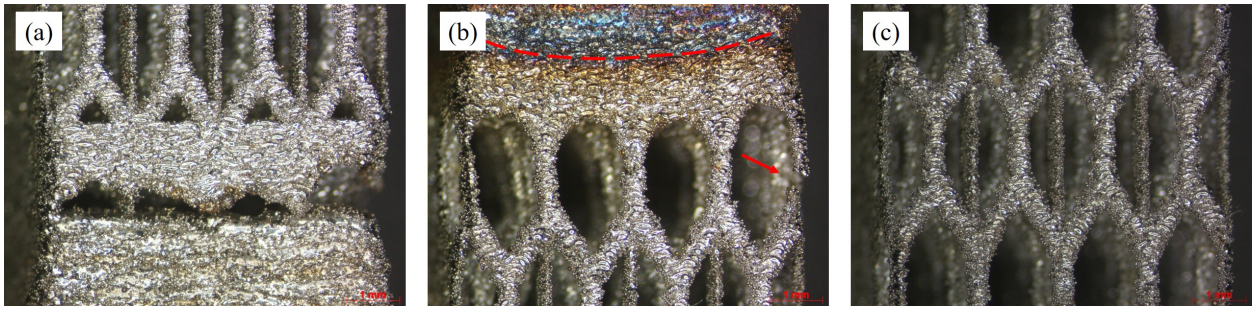

Figure 10. Macrograph of sample 6: (a) lower interface, (b) upper interface and (c) intermediate zone.

Finally, Fig. 11 provides a summarized representation of all the results obtained in the experiment. It can be observed that as P increases for a fixed value of v, the consolidation issue becomes less frequent. The opposite effect is observed with an increase in v. A higher frequency of consolidation issue occurrence was noticed in combinations of P and v that resulted in the lowest values of E_V within the tested range and, as E_V, increased, the issue became less frequent, as discussed previously. It is important to note that this result does not guarantee the failure of an eventual tensile test will occur within the intermediate zone, since it was possible to observe defects such as discontinuity of material on the lower interface in samples manufactured with E_V greater than 34,3 J/mm³.

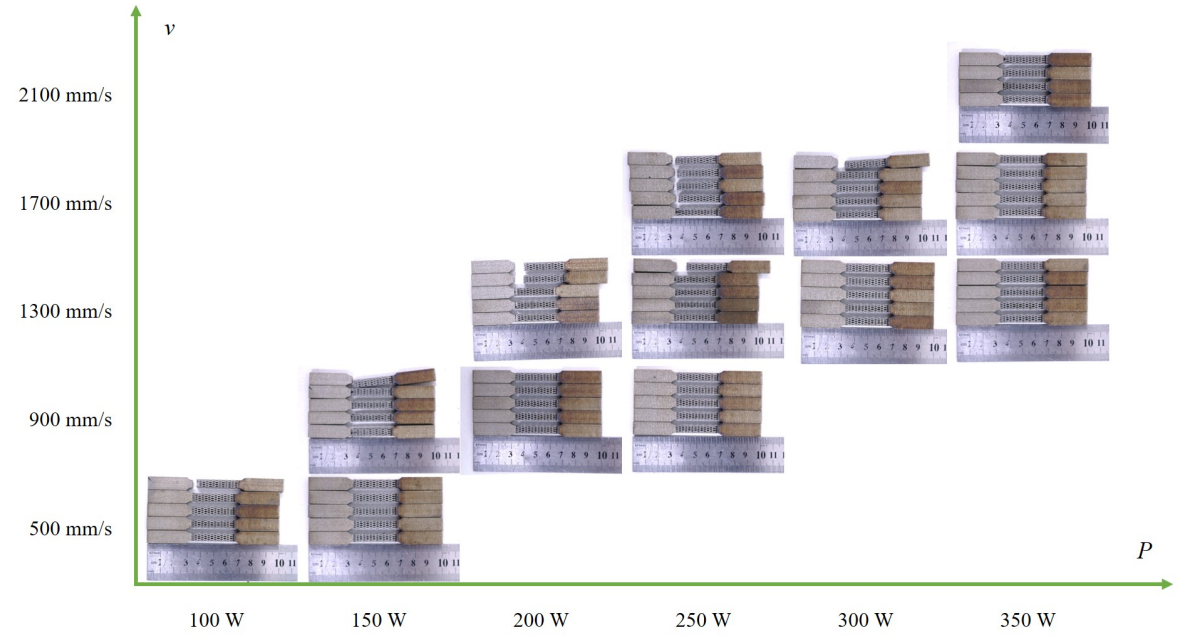

Figure 11. Summary of the results obtained according to P and v.

The mechanism that caused consolidation issues has mainly been attributed to residual stresses, an intrinsic effect of L-PBF processing. However, different responses in the quality of the interfaces were obtained by combining values of P and v. It is known that the sizing of scan line widths (w) is related to processing parameters P and v. Smaller values of w tend to weaken the interface regions between the support and the solid region. Besides, a decrease in w can also difficult heat dissipation, potentially increasing thermal gradients and further exacerbating residual stresses. Additionally, it is known that processing parameters influence the depth of the melt pool from each scanning line, which may have also impacted its consolidation (Denardi, 2021).

Regarding the overheating at the upper interface, a similar phenomenon has been described in the literature (Bobbio *et al.*, 2017; Lindecke *et al.*, 2018; Leary *et al.*, 2019). Figure 12 shows a scheme of this behavior. When the solid-support (lower) interface is printed, such as is represented in Fig. 12 (a), heat finds a much more favorable path for dissipation due to the greater area when compared to the support-solid (upper) interface is printed, such as is represented in Fig. 12 (b). In addition to that, the heat generated in the situation represented in Fig. 12 (b) is considerably higher over the situation represented in Fig. 12 (a) due to the higher area printed ($A_2 > A_1$ and $\dot{Q}_2 > \dot{Q}_1$). It is noteworthy to add that the metallic powder in this case acts as a thermal insulator because of the empty spaces between the particles.

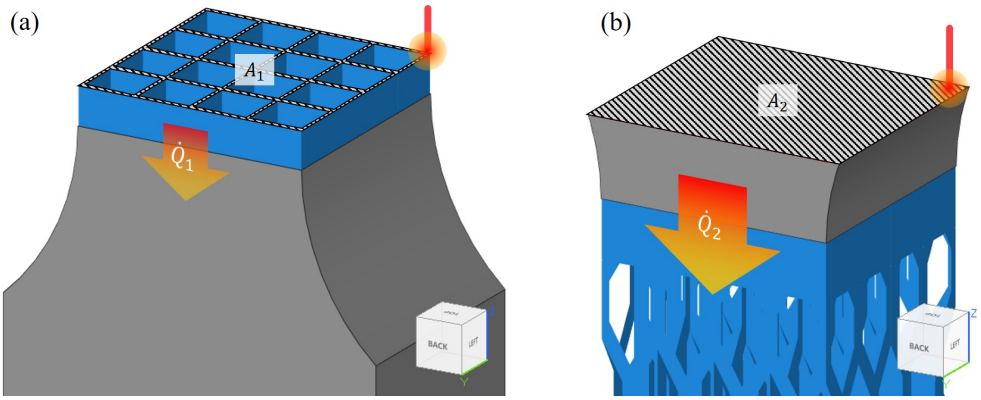

Figure 12. Overheating effect scheme: (a) solid-support (lower) interface and (b) support-solid (upper) interface.

To address the issues identified in this study, 3 different approaches were proposed: (1) adopt values for $[z]_o$ equivalent from 2 to 5 layers, particularly at the lower interface, to assist continuity between support and solid region and improve consolidation; (2) utilize $[xy]_o$ to guarantee that the support contour scanning path will be within the boundaries of the scanned slice when processing the solid region; and (3) implement additional auxiliary ligaments to withstand the loads generated by residual stresses and enhance heat dissipation from the upper towards the lower region in order to preserve the support structure, since it is the object of study. After processing, these ligaments can be cut via WEDM before conducting the tensile test.

5. CONCLUSION

Previous studies have examined the influence of design and processing parameters of support structures on warping, ease of removal, and tensile strength, offering valuable insights into their design and optimization. However, a lack of standardization in test specimens, evaluation methods, different material testing, and common objectives has hampered direct comparisons among studies. In light of these challenges, this work investigates the feasibility of manufacturing via L-PBF a standard support sample for tensile testing based on the subsize ASTM E8/E8M–16a specimen. The same design was printed with different combinations of laser power P and scanning speed v, and the impact of these combinations on the quality of the interface between support and solid regions was preliminarily analyzed.

After removing the powder from the build chamber and substrate, it was possible to observe that several samples exhibited issues in the lower interface between solid and support regions. Besides the consolidation issue, overheating and shrinkage in the solid region from the upper interface were also observed. Overall, the results showed that the consolidation depended on the processing parameters studied. When v was fixed, the consolidation improved as P increased. When P was fixed, the behavior was the opposite: as v increased, the consolidation worsened. When evaluating the impact of the processing parameters through the volumetric energy density E_V, consolidation issues were identified in samples produced with E_V lower than 34,3 J/mm³.

It is expected that both the results found in this study and the sample design proposed will be useful for engineers when characterizing the tensile strength of non-solid block-type support structures. In the following steps, it is intended to design and manufacture them as suggested previously.

6. REFERENCES

Aulus, R. and Bineli, R., 2011. "Direct Metal Laser Sintering (DMLS)". *Current Advances in Mechanical Design and Production VII*, p. 7.

Bartsch, K., Ohrenberg, J. and Emmelmann, C., 2020. "Benchmark parts for the evaluation of optimized support structures in Laser Powder Bed Fusion of metals". *Procedia CIRP*, Vol. 94, pp. 254–259.

Bassoli, E., Sola, A., Celesti, M., Calcagnile, S. and Cavallini, C., 2018. "Development of laser-based powder bed fusion process parameters and scanning strategy for new metal alloy grades". *Materials*, Vol. 11, p. 2356.

Bayoumi, A., 2000. "Design for manufacture and assembly (DFMA)". *Current Advances in Mechanical Design and Production VII*, pp. 501–509.

Bobbio, L., Qin, S., Dunbar, A., Michaleris, P. and Beese, A., 2017. "Characterization of the strength of support structures used in powder bed fusion additive manufacturing of Ti-6Al-4V". *Additive Manufacturing*, Vol. 14, pp. 60–68.

Calignano, F., 2014. "Design optimization of supports for overhanging structures in aluminum and titanium alloys by selective laser melting". *Materials & Design*, Vol. 64, pp. 203–213. ISSN 0261–3069.

DebRoy, T., Wei, H., Zuback, J., Mukherjee, T., Elmer, J., Milewski, J., Beese, A., Wilson-Heid, A., De, A. and Zhang, W., 2018. "Additive manufacturing of metallic components – process, structure and properties". *Progress in Materials Science*, Vol. 92, pp. 112–224.

Denardi, B., 2021. *Otimização de Parâmetros do Processo de Manufatura Aditiva Por Fusão em Leito de Pó a Laser da Liga AISI 316L com Foco em Produtividade e Propriedades Mecânicas*. Master's thesis, Universidade Tecnológica Federal do Paraná – UTFPR, Curitiba, PR.

Gallego, D.A., Oliveira, H.R., Chastinet, V.L., Borges, D.G., Bento, M.V., Denardi, B. and Forni, R., 2022. "Application of design for additive manufacturing focused on spare parts using laser powder bed fusion". *Rio Oil & Gas Expo and Conference 2022*, Vol. 21, No. 429, pp. 1–14. ISSN 2525–7579.

Jiang, J., Xu, X. and Stringer, J., 2018. "Support structures for additive manufacturing". *Journal of Manufacturing and Materials Processing*, Vol. 2, No. 4, pp. 1–23. ISSN 2504–4494.

Leary, M., Maconachie, T., Sarker, A., Faruque, O. and Brandt, M., 2019. "Mechanical and thermal characterisation of AlSi10Mg SLM block support structures". *Materials & Design*, Vol. 183, p. 108138.

Lindecke, P., Blunk, H., Wenzl, J., MÖller, M. and Emmelmann, C., 2018. "Optimization of support structures for the laser additive manufacturing of TiAl6V4 parts". *Procedia CIRP*, Vol. 74, pp. 53–58.

Liu, Y., Zhang, M., Shi, W., Ma, Y. and Yang, J., 2021. "Study on performance optimization of 316L stainless steel parts by High-Efficiency Selective Laser Melting". *Optics and Laser Technology*, Vol. 138, pp. 1–11.

Munhoz, A., Larosa, M., Longhitano, G., Bineli, A., Zavaglia, C. and Silva, J., 2017. "Processos de AM por fusão de leito de pó metálico". In N. Volpato, ed., *Manufatura aditiva: tecnologias e aplicações da impressão 3D*, Editora Blucher, São Paulo, São Paulo, Brasil, pp. 248–271. ISBN 9788521211518.

Oliveira, J., Lalonde, A. and Ma, J., 2020. "Processing parameters in laser powder bed fusion metal additive manufacturing". *Materials & Design*, Vol. 193, pp. 1–12.

Schmitt, M., Kempter, B., Schlick, G. and Reinhart, G., 2020. "Parameter identification approach for support structures in laser powder bed fusion and analysis of influencing factors". *Procedia CIRP*, Vol. 94, pp. 260–265.

Sefene, E.M., 2022. "State-of-the-art of selective laser melting process". *Journal of Manufacturing Systems*, Vol. 63, pp. 250–274. ISSN 0278–6125.

Sun, S., Brandt, M. and Easton, M., 2017. "Powder bed fusion processes: An overview". In M. Brandt, ed., *Laser Additive Manufacturing*, Woodhead Publishing, Woodhead Publishing Series in Electronic and Optical Materials, pp. 55–77. ISBN 978-0-08-100433-3.

Tan, C., Li, S., Essa, K., Jamshidi, P., Zhou, K., Ma, W. and Attallah, M., 2019. "Laser powder bed fusion of Ti-rich TiNi lattice structures". *International Journal of Machine Tools and Manufacture*, Vol. 141, pp. 19–29. ISSN 0890–6955.

Volpato, N. and de Carvalho, J., 2017. "Introdução à Manufatura Aditiva ou Impressão 3D". In N. Volpato, ed., *Manufatura aditiva: tecnologias e aplicações da impressão 3D*, Editora Blucher, São Paulo, São Paulo, Brasil, pp. 16–31. ISBN 9788521211518.

Wang, Z., Guan, K., Gao, M., Li, X., Chen, X. and Zeng, X., 2012. "The microstructure and mechanical properties of deposited-IN718 by selective laser melting". *Journal of Alloys and Compounds*, Vol. 513, No. 5, pp. 518–523. ISSN 0925–8388.

Weber, S., Montero, J., Bleckmann, M. and Paetzold, K., 2020. "Parameters on support structure design for metal additive manufacturing". *Proceedings of the Design Society: Design Conference*, Vol. 1, pp. 1145–1154.

Zhu, L., Feng, R., Xi, J., Li, P. and Wei, X., 2019. "A Lightweight Design of Tree-shaped Support Structures for SLM Additive Manufacturing". *Computer-Aided Design and Applications*, Vol. 17, pp. 716–726.

7. RESPONSIBILITY NOTICE

The authors are solely responsible for the printed material included in this paper.